CARBON letters

Note

Carbon Letters Vol. 23, 69-73 (2017)

Lyocell-based activated carbon fibers improved the adsorption of harmful gas properties when produced via dual-simultaneous treatments

Byong Chol Bai[1,2], Ji Sun Im[1,2,♠] and Young-Seak Lee[3,♠]

[1]C-Industry Incubation Center, Korea Research Institute of Chemical Technology (KRICT), Daejeon 34114, Korea
[2]University of Science and Technology (UST), Daejeon 34113, Korea
[3]Department of Applied Chemistry and Biological Engineering, Chungnam National University, Daejeon 34134, Korea

Article Info

Received 28 April 2017
Accepted 22 May 2017

♠Corresponding Author
E-mail: jsim@krict.re.kr
E-mail: youngslee@cnu.ac.kr
Tel: +82-42-860-7366
Tel: +82-42-821-7007

Open Access

DOI: http://dx.doi.org/10.5714/CL.2017.23.069

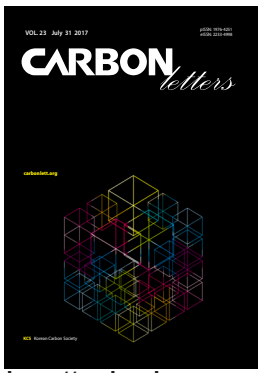

http://carbonlett.org

pISSN: 1976-4251
eISSN: 2233-4998

In gas adsorption processes, activated carbon fibers (ACFs) are used for the adsorption of the harmful gases that are generated by coal or oil combustion, and they have been widely studied [1,2]. ACFs have been used for harmful gas removal because of their specific surface area, micropores, reproducibility, safety, and processing ability, which are beneficial properties for a wide range of applications [3,4].

Cellulose fibers are important carbon fiber precursors due to their low metal ion content, low density, and ease of production. Cellulose fibers degrade at high temperatures. Specifically, upon heating, they undergo a series of interrelated physical and chemical changes. These reactions are accelerated in the presence of various organic or inorganic catalysts and Lewis acids that catalyse the dehydration reactions [5]. Therefore, the excellent flame-retardant properties of cellulose fibers can be modified by these reactions. This treatment induces a slow process of dehydration, rearrangement, carbonyl group formation, and CO and CO_2 evolution. Additionally, it promotes the formation of a carbonaceous residue that enhances the flame-retardant behaviour of cellulose fibers [6].

Harmful gas adsorption research, especially on SO_2 adsorption, has been focused on developing materials that have basic nitrogen groups [7]. Previous studies have examined the chemical effects of the observed correlation between the SO_2 capacity and the surface basicity [8]. Furthermore, nitrogen-treated ACFs were shown to have high stability of the aromatic nitrogen groups without a significant decrease in the SO_2 adsorption capacity [9].

In this study, nitrogen-treated ACFs were used to fabricate a harmful gas adsorption matrix by using dual-simultaneous treatments. These methods can produce ACFs and develop nitrogen functional groups simply and simultaneously. First, to enhance the gas adsorption properties of the Lyocell-based ACFs, a porous structure was developed by using the di-ammonium-hydrogen phosphate (DAHP) phosphorus compound that is used in highly flame-retardant media. Second, for the simultaneous treatment to enhance the gas adsorption properties of ACFs, we used urea to develop nitrogen functional groups on the ACFs surfaces without significantly changing their properties. Here, the changes in the textural and adsorption properties were obtained via pyrolysis of the Lyocell fibers, followed by DAHP and urea treatment at low temperatures. These dual-simultaneous treatments can induce high selectivity and adsorption of harmful gases.

In this study, Lyocell fibers with a length of 20 cm and an approximate weight of 10 g (Kolon Industries Co., Korea) were used. For the chemical treatment, DAHP (Sigma-Aldrich Co., USA) was chosen as the agent for chemical activation and flame-retardant treatment [10] to develop a porous structure. Additionally, urea (>99.0%; Samchun Chemical, Korea) was used as a chemical treatment agent for the development of ACFs with basic nitrogen groups on their surfaces.

For the dual-simultaneous treatment, first, 10 g of raw Lyocell fibers was immersed in 100 mL of a 7 wt% DAHP solution for 5 h at 60°C. These optimal chemical treatment conditions were determined based on our previous work [6]. After the fibers were treated, the solution was removed and dried overnight in a vacuum oven at 70°C. Dried Lyocell fibers

were immersed in 100 mL of a urea solution (50 g urea dissolved in distilled water) and sonicated for 1 h at room temperature. After the second treatment, the excess solution was removed by centrifugation.

The dual-simultaneous-treated Lyocell fibers were placed in an alumina boat within a reactor. The dual-simultaneous-treated ACF samples are hereafter referred to as NLA_4, NLA_5, and NLA_6, according to their heating temperatures of 400, 500, and 600°C, respectively; the heating was performed for 1 h in a nitrogen atmosphere. The heating rate was 10°C/min, and the nitrogen feed rate was 100 mL/min. After activation, the ACFs were washed with distilled water to remove the unreacted urea and were dried overnight in a vacuum oven at 70°C.

The textural properties of the prepared ACFs were investigated. The ACF samples were heated under vacuum conditions at 150°C for 8 h to remove the water and some of the impurities that were adsorbed in the samples prior to the analysis. We used Brunauer-Emmett-Teller (BET) analysis (ASAP2020 instrument; Micromeritics Co. in Korea Research Institute of Chemical Technology [KRICT], Korea) to investigate the specific surface area, total pore volume, pore size distribution (PSD), and micropore fraction. Elemental analysis of the ACFs was performed using an organic elemental analyser (Thermo Scientific FLASH EA-2000 in KRICT). We also evaluated the N/C ratio of the ACFs, and the results are presented in Table 1. To observe the surface characteristics and microstructure of the manufactured samples, an analysis was carried out using an ultra high resolution field emission scanning electron microscope (UHR FE-SEM, Hitachi, Japan; S-5500, in Korea Basic Science Institute [KBSI] Jeonju Center). A thermogravimetric analysis (TGA; Shimadzu TGA-50H thermo analyzer in KRICT) was carried out at a heating rate of 5°C/min and with temperatures as high as 900°C in an N_2 atmosphere.

The SO_2 adsorption experiments were performed as follows. First, 0.1 g of ACFs was placed in a vertical stainless steel reactor with an internal diameter of 5 mm. To measure the internal bed temperature, a thermocouple was placed 1 mm above the ACFs. The total flow was maintained at 1500 cc/min, and the SO_2 concentration was approximately 40 ppm; the analyser continuously monitored the weight gain. The outlet SO_2 gas concentrations were continuously measured using a multi-gas detector (Teledyne model 7600 device in KRICT), with the concentrations recorded every 1 s.

To analyse the SO_2 adsorption in the fixed bed reactor, breakthrough and saturation curves (C_t/C_0 vs. time) were plotted, and the data were evaluated using the following equations [11]:

$$V_{eff} = Q \cdot t_{total,}$$

where V_{eff} is effluent volume, Q is the volumetric flow rate (mL/min) and t_{total} is the time of SO_2 adsorption.

The total uptake capacity (q_{total}, mg) is given by [12]

$$q_{total} = \frac{Q}{1000}\int_{t=0}^{t=t_{total}} C\,dt$$

where C is the concentration of each point for the SO_2 gas.

The total amount of SO_2, m_{total} (mg), transported to the reactor and the total SO_2 removal (R_{total}, %) were calculated according to [13]:

$$m_{total} = \frac{C_0 V_{eff}}{1000}$$

$$R_{total} = \frac{q_{total}}{m_{total}} \times 100$$

Fig. 1 shows the effects of the DAHP treatment on the thermal resistance of Lyocell fibers using the TGA curve obtained

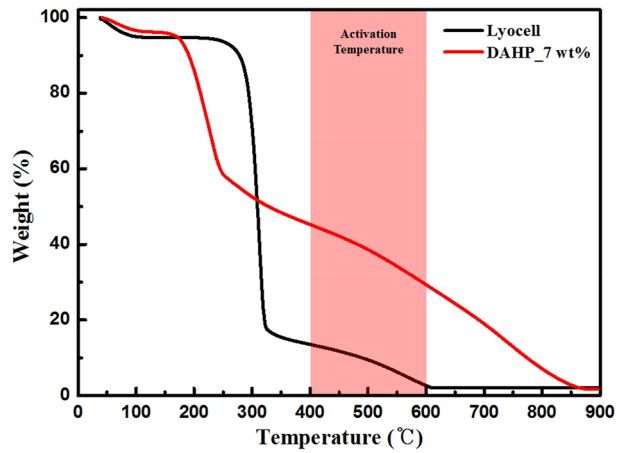

Fig. 1. Thermogravimetric analysis curves of un-treated and treated Lyocell fibers. DAHP, di-ammonium-hydrogen phosphate.

Table 1. Carbon yield and elemental analysis parameters of the Lyocell fiber and ACFs

Sample	Chemical activation		Elemental analysis (%)				
	Temperature (°C)	Yield (%)	C	H	N	O	N/C
Lyocell	-	-	41.0	6.3	-	52.7	-
LA_6[a)]	600	44.5	83.0	0.8	-	16.2	-
NLA_4	400	53.3	75.0	3.2	3.1	18.7	4.13
NLA_5	500	48.7	78.8	2.1	4.5	14.6	5.71
NLA_6	600	42.0	85.1	1.0	5.1	8.8	5.99

ACFs, activated carbon fibers.
[a)]Non-urea-treated Lyocell-based ACFs.

under the nitrogen atmosphere at a heating rate of 10°C. It is known that the DAHP treatment will significantly lower the decomposition temperature of a Lyocell fiber. In Fig. 1, the 7 wt% DAHP treatment Lyocell fibers show the maximum weight loss point on the TGA curve, at 205°C, which is 90°C lower than that of the un-treated fibers. A slight slope changes in the TGA curve observed for the DAHP-treated Lyocell fibers appears as the two main curves, which we refer to as steps 1 and 2. The curve at approximately 200°C (step 1) is due to the thermal decomposition of DAHP. After decomposition, Lyocell fibers released water and ammonia by the phosphorylation reaction [14]. Moreover, the DAHP altered the profile of step 2, which was shifted to a higher temperature and became broader, thus changing the combustion pathway. The char yields of the DAHP-modified Lyocell fibers tended to increase. The improved char yield was likely caused by the esterification of the phosphoric acid (H_3PO_4) and the primary hydroxyl groups in the fiber during the thermal decomposition of DAHP [15]. An increasing char yield implies a greater fire resistance of the sample, as it was proposed that the char formation would limit the production of combustion gases, inhibit the combustion gases from diffusing to the pyrolysis zone, and protect the material surface from heat and air [16].

Fig. 2 shows surface images of the manufactured sample. The surface roughness of the non-activated Lyocell fiber was observed to be smooth, and the average diameter was approximately 13±1.0 μm. Following activation, the average diameter of the ACFs was approximately 8±1.0 μm because the Lyocell fibers were degraded at the activation temperatures. It was confirmed that some of the unreacted urea was quite uniformly dispersed over the surface of the NLA_4 and NLA_5 samples. Additionally, it was observed that the amount of the unreacted urea that impregnated the surface decreased as the activation temperature increased. It is noteworthy that the amount, dispersion, and aggregation of the urea all significantly influenced the morphologies of the ACFs. It appears that some ACF pores can be blocked in the presence of urea, resulting in a specifically decreased surface area.

Elemental analysis was performed to compare the chemical compositions at the surfaces of the non-urea-treated and dual-simultaneous-treated ACFs, and the results are given in Table 1. The N content in the dual-simultaneous-treated ACFs was greater than that in the non-urea-treated ACFs, increasing the N/C ratio of 0.00 to 5.99. This can be explained by the reaction mechanism between the oxygen group at the Lyocell surface and the urea. In this type of reaction, urea will easily react both at the edge and inside the pores of the cellulose surface, which has oxygen groups that act as chemical defects [17]. During the dual-simultaneous treatment, active sites were effectively introduced on the surfaces of the Lyocell fibers by the ionized urea molecules. However, the observed trend of an increase with respect to temperature may be attributed to the increased electron energy of the urea molecules because more urea molecules are involved in the reaction with oxygen groups in the Lyocell fiber at high temperatures.

The pore textures of the ACFs were investigated by a nitrogen adsorption analysis at –196°C. A summary of the textural properties of the non-urea-treated and dual-simultaneous-treated ACFs is presented in Table 2. The BET specific surface area and pore volume were increased after the heat treatment. In particular, the specific surface area of NLA_6 was increased by approximately 562 up to 809 m^2/g, compared to NLA_4, which is activated at 400°C. Additionally, the pore volume was increased by the activation. Sample NLA_6 exhibits the highest total pore

Table 2. Textural characteristics of the non-urea-treated and dual-simultaneous-treated ACFs

Sample	BET surface area (m^2/g)	DR-V_{micro} (cm^3/g)	BJH-V_{meso} (cm^3/g)	V_{total} (cm^3/g)
LA_6[a)]	845	0.301	0.045	0.346
NLA_4	562	0.218	0.048	0.266
NLA_5	723	0.289	0.033	0.322
NLA_6	809	0.329	0.028	0.357

ACFs, activated carbon fibers; BET, Brunauer-Emmett-Teller; DR, Dubinin Radushkevich; BJH, Barrett-Joyner-Halenda.
[a)]Non-urea-treated Lyocell-based ACFs.

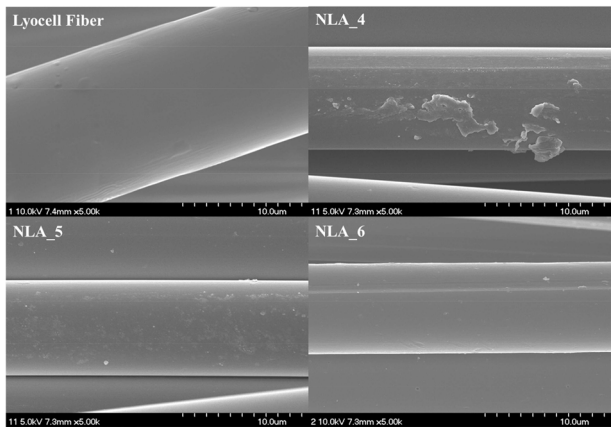

Fig. 2. Field emission scanning electron microscope images of the Lyocell fiber and dual-simultaneous-treated activated carbon fibers.

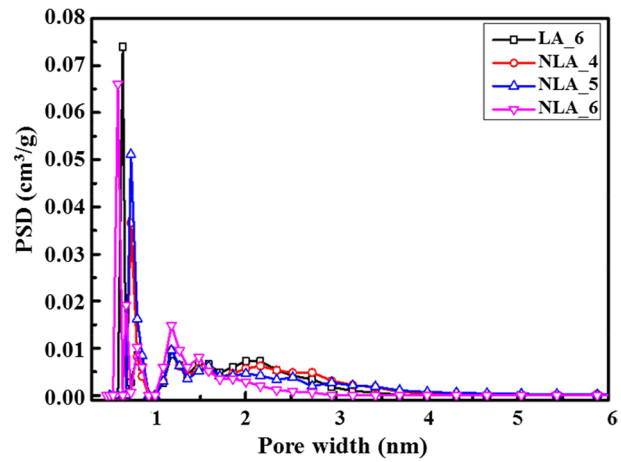

Fig. 3. Pore size distribution (PSD) of the volume of the non-urea-treated and dual-simultaneous-treated activated carbon fibers.

Table 3. Characteristic parameters obtained from SO_2 adsorption breakthrough curves

Sample	Superficial velocity	Initial concentration	Bed height	Total time	Breakthrough time	Saturation time	Effluent volume	Total amount removed	Total removal	Adsorption capacity
	Q (cc/min)	C_0 (mg/L)	Z (cm)	t_{total} (min)	$t_{0.05}$ (min)	$t_{0.95}$ (min)	V_{eff} (cc)	m_{total} (mg)	R_{total} (%)	q_{total} (mg)
*LA_6	1500	40.00	2	31.98	3.82	13.54	47,970	1918.8	31.37	601.88
NLA_4	1500	40.00	2	30.12	3.32	11.89	45,180	1807.2	31.68	572.52
NLA_5	1500	40.00	2	34.81	5.28	17.79	52,215	2088.6	42.70	891.77
NLA_6	1500	40.00	2	40.39	6.21	19.88	60,585	2423.4	47.99	1163.09

*Non-urea-treated Lyocell-based activated carbon fibers.

volume among the dual-simultaneous-treated ACFs, with a pore volume of 0.339 cm^3/g. Fig. 3 shows the PSD of the non-urea-treated and dual-simultaneous-treated ACFs. The pore diameters are found mainly in the 1–4 nm pore range. The origin of the shifted micropore peak position of NLA_6 is aggregation of the urea with the ACFs during the chemical reaction. Therefore, the micropore fraction of NLA_6 increased despite the increase of the total pore volume and specific surface area.

The breakthrough time, saturation time, total removal, and SO_2 adsorption capacity values were obtained using the above formulas, and the results are shown in Table 3. In real applications, one of the main advantages of a simulation model is its capacity to predict the breakthrough time (t_b) and the saturation time (t_s). In this study, t_b and t_s were defined somewhat arbitrarily as the times corresponding to C/C_0=5%, but this value can be changed according to the specific requirements [18,19]. The data in Table 3 show that the SO_2 adsorption properties increased in the order of NLA_4<LA_6<NLA_5<NLA_6. These results are attributed to the effect of the nitrogen atoms in the urea structure when the urea support was chemically bound to the ACF surface [20]. Furthermore, the NLA_6 sample exhibited the highest values among the results for all samples. As the adsorption capacity of SO_2 increased from 572.52 to 1163.09 mg, the breakthrough and saturation times increased from 3.32 to 6.21 min and from 11.89 to 19.88 min, respectively.

In the presence of nitrogen functional groups, it appears that reactive SO_2 was formed on the surfaces of the ACFs. According to various studies [21-23], surface nitrogen species (RC(N), R denotes carbon surface) acting as catalytic active centres may facilitate the formation of SO_2^- (lone pair electron) due to the extra π electrons, according to (1):

$$RC(N^+ - e^-) + SO_2 \rightarrow RC(N^+ - SO_2^-) \quad (1)$$

This mechanism is one of the transitional conversion steps from SO_2 to SO_3. According to this mechanism, the nitrogen active site plays an important role in the adsorption of SO_2 on the ACFs. This phenomenon occurs when extra π electrons are present on the nitrogen in the higher energy state, and SO_2 molecules are transferred to the carbon pores when active sites are introduced on the ACF surfaces [24]. Therefore, it is likely that it can interact with the SO_2 molecules, which have lone pair electrons. Based on these results, the urea structure interacted strongly with the SO_2 molecules and thereby helped adsorb the SO_2 gas and changed the electrical resistance easily via the electron hopping effect.

Conflict of Interest

No potential conflict of interest relevant to this article was reported.

Acknowledgements

This work was supported by the Korea Evaluation Institute of Industrial Technology (KEIT) (Grant No. 10045669).

References

[1] Kim JY, Lee JG, Hong IP. NO reduction and oxidation over PAN based-ACF. Carbon Lett, **1**, 17 (2000).

[2] Sumathi S, Bhatia S, Lee KT, Mohamed AR. Optimization of microporous palm shell activated carbon production for flue gas desulphurization: experimental and statistical studies. Bioresour Technol, **100**, 1614 (2009). https://doi.org/10.1016/j.biortech.2008.09.020.

[3] Tseng HH, Wey MY, Fu CH. Carbon materials as catalyst supports for SO_2 oxidation: catalytic activity of CuO-AC. Carbon, **41**, 139 (2003). https://doi.org/10.1016/s0008-6223(02)00264-6.

[4] Lua AC, Yang T. Theoretical and experimental SO_2 adsorption onto pistachio nut-shell activated carbon for a fixed-bed column. Chem Eng J, **155**, 175 (2009). https://doi.org/10.1016/j.cej.2009.07.031.

[5] Lisovskii A, Semiat R, Aharoni C. Adsorption of sulfur dioxide by active carbon treated by nitric acid: I. Effect of the treatment on adsorption of SO_2 and extractability of the acid formed. Carbon, **35**, 1639 (1997). https://doi.org/10.1016/s0008-6223(97)00129-2.

[6] Bai BC, Kim EA, Jeon YP, Lee CW, In SJ, Lee YS, Im JS. Improved flame-retardant properties of lyocell fiber achieved by phosphorus compound. Mater Lett, **135**, 226 (2014). https://doi.org/10.1016/j.matlet.2014.07.131.

[7] Heo YJ, Le MUT, Park SJ. Investigation of carbon dioxide adsorption by nitrogen-doped carbons synthesized from cubic MCM-48 mesoporous silica. Carbon Lett, **18**, 62 (2016). https://doi.

org/10.5714/cl.2016.18.062.

[8] Kang SC, Im JS, Lee YS. Improved sensitivity of an NO gas sensor by chemical activation of electrospun carbon fibers. Carbon Lett, **12**, 21 (2011). https://doi.org/10.5714/cl.2011.12.1.021.

[9] Park MS, Lee S, Jung MJ, Kim HG, Lee YS. NO gas sensing ability of activated carbon fibers modified by an electron beam for improvement in the surface functional group. Carbon Lett, **20**, 19 (2016). https://doi.org/10.5714/cl.2016.20.019.

[10] Tang MM, Bacon R. Carbonization of cellulose fibers I. Low temperature pyrolysis. Carbon, **2**, 211 (1964). https://doi.org/10.1016/0008-6223(64)90035-1.

[11] Vijayaraghavan K, Jegan J, Palanivelu K, Velan M. Batch and column removal of copper from aqueous solution using a brown marine alga Turbinaria ornate. Chem Eng J, **106**, 177 (2005). https://doi.org/10.1016/j.cej.2004.12.039.

[12] Aksu Z, Gönen F. Biosorption of phenol by immobilized activated sludge in a continuous packed bed: prediction of breakthrough curves. Process Biochem, **39**, 599 (2004). https://doi.org/10.1016/s0032-9592(03)00132-8.

[13] Hasana SH, Srivastavaa P, Talatb M. Biosorption of lead using immobilized Aeromonas hydrophila biomass in up flow column system: factorial design for process optimization. J Hazardous Mater, **177**, 312 (2010). https://doi.org/10.1016/j.jhazmat.2009.12.034.

[14] Statheropoulos M, Kyriakou SA. Quantitative thermogravimetric-mass spectrometric analysis for monitoring the effects of fire retardants on cellulose pyrolysis. Anal Chim Acta, **409**, 203 (2000). https://doi.org/10.1016/s0003-2670(99)00859-4.

[15] Grønli MG, Várhegyi G, Di Blasi C. Thermogravimetric analysis and devolatilization kinetics of wood. Ind Eng Chem Res, **41**, 4201 (2002). https://doi.org/10.1021/ie0201157.

[16] Nam S, Condon BD, Parikh DV, Zhao Q, Cintrón MS, Madison C. Effect of urea additive on the thermal decomposition of greige cotton nonwoven fabric treated with diammonium phosphate. Polym Degrad Stab, **96**, 2010 (2011). https://doi.org/10.1016/j.polymdegradstab.2011.08.014.

[17] Huang MR, Li XG. Thermal degradation of cellulose and cellulose esters. J Appl Polym Sci, **68**, 293 (1998). https://doi.org/10.1002/(sici)1097-4628(19980411)68:2<293::aid-app11>3.0.co;2-z.

[18] Futalan CM, Kan CC, Dalida ML, Pascua C, Wan MW. Fixed-bed column studies on the removal of copper using chitosan immobilized on bentonite. Carbohydr Polym, **83**, 697 (2011). https://doi.org/10.1016/j.carbpol.2010.08.043.

[19] Serna-Guerrero R, Sayari A. Modeling adsorption of CO_2 on amine-functionalized mesoporous silica. 2: Kinetics and breakthrough curves. Chem Eng J, **161**, 182 (2010). https://doi.org/10.1016/j.cej.2010.04.042.

[20] Yoosefian M, Zahedi M, Mola A, Naserian S. A DFT comparative study of single and double SO_2 adsorption on Pt-doped and Au-doped single-walled carbon nanotube. Appl Surf Sci, **349**, 864 (2015). https://doi.org/10.1016/j.apsusc.2015.05.088.

[21] Matzner R, Boehm HP. Influence of nitrogen doping on the adsorption and reduction of nitric oxide by activated carbons. Carbon, **36**, 1697 (1998). https://doi.org/10.1016/s0008-6223(98)90047-1.

[22] Schmiers H, Friebel J, Streubel P, Hesse R, Kopsel R. Change of chemical bonding of nitrogen of polymeric N-heterocyclic compounds during pyrolysis. Carbon, **37**, 1965 (1999). https://doi.org/10.1016/s0008-6223(99)00071-8.

[23] Strelko VV, Kutz VS, Thrower PA. On the mechanism of possible influence of heteroatoms of nitrogen, boron and phosphorus in a carbon matrix on the catalytic activity of carbons in electron transfer reactions. Carbon, **38**, 1499 (2000). https://doi.org/10.1016/s0008-6223(00)00121-4.

[24] Foley HC. Carbogenic molecular sieves: synthesis, properties and applications. Microporous Mater, **4**, 407 (1995). https://doi.org/10.1016/0927-6513(95)00014-z.